Available online at www.sciencedirect.com
ScienceDirect
Journal of Power Sources 173 (2007) 943–949
JOURNAL OF POWER SOURCES
www.elsevier.com/locate/jpowsour

Hydrogen production by steam reforming of liquefied natural gas over a nickel catalyst supported on mesoporous alumina xerogel

Jeong Gil Seo, Min Hye Youn, Kyung Min Cho, Sunyoung Park, In Kyu Song *

School of Chemical and Biological Engineering, Research Center for Energy Conversion and Storage, Seoul National University, Shinlim-dong, Kwanak-ku, Seoul 151-744, South Korea

Received 1 April 2007; received in revised form 1 August 2007; accepted 6 August 2007
Available online 1 September 2007

Abstract

Mesoporous alumina xerogel (A-SG) is prepared by a sol–gel method for use as a support for a nickel catalyst. The Ni/A-SG catalyst is then prepared by an impregnation method, and is applied to hydrogen production by steam reforming of liquefied natural gas (LNG). The effect of the mesoporous alumina xerogel support on the catalytic performance of Ni/A-SG catalyst is investigated. For the purpose of comparison, a nickel catalyst supported on commercial alumina (A-C) is also prepared by an impregnation method (Ni/A-C). Both the hydroxyl-rich surface and the electron-deficient sites of the A-SG support enhance the dispersion of the nickel species on the support during the calcination step. The formation of the surface nickel aluminate phase in the Ni/A-SG catalyst remarkably increases the reducibility and stability of the catalyst. Furthermore, the high-surface area and the well-developed mesoporosity of the Ni/A-SG catalyst enhance the gasification of surface hydrocarbons that are adsorbed in the reaction. In the steam reforming of LNG, the Ni/A-SG catalyst exhibits a better catalytic performance than the Ni/A-C catalyst in terms of LNG conversion and hydrogen production. Moreover, the Ni/A-SG catalyst shows strong resistance toward catalyst deactivation.

Keywords: Alumina xerogel; Nickel catalyst; Sol–gel method; Liquefied natural gas; Steam reforming; Hydrogen production

1. Introduction

Catalytic steam reforming of methane has been extensively studied for the production of hydrogen or synthesis gas [1–4]. Liquefied natural gas (LNG), which is abundant and mainly composed of methane, can serve as an alternative source for hydrogen production by steam reforming. The LNG pipelines may become more widespread in the future, which will make LNG well suited as a hydrogen source for residential reformers in fuel cell applications.

Conventional nickel-based catalysts such as Ni/Al_2O_3 suffer from severe catalyst deactivation in the steam reforming reactions due to carbon deposition and metal sintering [5–9]. Therefore, nickel-based catalysts require a high reaction temperature and an excess amount of steam to prevent coke deposition on the catalyst surfaces during steam reforming [1–3]. Such severe reaction conditions for hydrogen production are not, however, favourable for the efficient operation of fuel cell systems. Therefore, low-temperature reforming technology has attracted much attention because of its potential applicability in fuel cell systems such as the polymer electrolyte membrane fuel cell (PEMFC) [10–12]. At low temperatures, however, it is very difficult to reduce the supported nickel catalyst due to the strong interaction between nickel and support [13,14]. Thus, developing an efficient catalyst with high activity and high durability is required for both on-site and off-site hydrogen production by steam reforming. Although noble metals such as rhodium and ruthenium are known to be very active in steam reforming reactions, nickel-based catalysts can be a practical alternative if properly designed.

The catalytic performance of a supported nickel catalyst in steam reforming reactions depends strongly on the chemical and textural properties of the support. Therefore, modification of an appropriate support for a nickel catalyst can be a feasible route to improve the catalytic performance of a supported nickel catalyst. Many attempts have been made to modify the support for a nickel catalyst [15–20]. For example, it has been reported that the addition of alkali and alkali earth metal oxides

* Corresponding author. Tel.: +82 2 880 9227; fax: +82 2 889 7415.
E-mail address: inksong@snu.ac.kr (I.K. Song).

0378-7753/$ – see front matter © 2007 Elsevier B.V. All rights reserved.
doi:10.1016/j.jpowsour.2007.08.064

into an Al_2O_3 support improve the coke resistance of a supported nickel catalyst by enhancing the gasification reaction in the steam reforming of methane [21–23]. Ni–alumina catalysts prepared by a sol–gel method [24–27] have also been investigated in reforming reactions with the aim of suppressing carbon deposition [28–30].

Metal oxides prepared by a sol–gel method retain hydroxyl-rich surfaces, and therefore, exhibit unique textural and chemical properties compared with those prepared by a conventional method. In particular, alumina materials prepared by a sol–gel method have high surface areas and controllable textural and chemical properties. It was reported that an alumina aerogel with a well-developed pore structure inhibited carbon deposition in the CO_2 reforming of methane, and this resulted in enhancement of both methane conversion and coke resistance [28,30]. The role and effect of an alumina xerogel support on catalytic performance in either a CO_2 reforming or a steam reforming reaction has not, however, been clearly investigated. Therefore, developing a sol–gel derived alumina xerogel support for a nickel catalyst in hydrogen production by the steam reforming of LNG is of great interest.

In this work, an alumina xerogel is prepared by a sol–gel method for use as a support for a nickel catalyst. A Ni/Al_2O_3 catalyst is then prepared by an impregnation method, and is applied to hydrogen production by steam reforming of LNG. The effect of the alumina xerogel support on the catalytic performance of Ni/Al_2O_3 is investigated.

2. Experimental

2.1. Preparation of alumina xerogel support and Ni/Al_2O_3 catalyst

An alumina xerogel support was prepared by a sol–gel method, according to the similar method reported in the literature [28,30,31]. A known amount of aluminum precursor (aluminum *sec*-butoxide, Sigma–Aldrich) was dissolved in ethanol at 80 °C with vigorous stirring. For the partial hydrolysis of the aluminum precursor, small amounts of nitric acid and distilled water, which had been diluted with ethanol, were slowly added to the solution containing the aluminum precursor. After maintaining the resulting solution at 80 °C for a few minutes, a clear sol was obtained. The sol was then cooled to room temperature with vigorous stirring. A transparent monolithic gel was formed within a few minutes by adding an appropriate amount of water diluted with ethanol to the sol. After ageing the alumina gel for 24 h, it was dried overnight at 120 °C. The resulting powder was finally calcined at 700 °C for 5 h to yield the alumina xerogel support. The prepared alumina xerogel support is denoted as A-SG.

A nickel catalyst supported on alumina xerogel was prepared by impregnating a known amount of nickel precursor ($Ni(NO_3)_2{\cdot}6H_2O$, Sigma–Aldrich) on the alumina xerogel support. The prepared Ni/Al_2O_3 catalyst is denoted as Ni/A-SG. For the purpose of comparison, a nickel catalyst supported on commercial Al_2O_3 (Degussa, denoted as A-C) was also prepared by an impregnation method. The nickel catalyst supported on commercial Al_2O_3 is denoted as Ni/A-C. The nickel loading was fixed at 20 wt.% in both cases.

2.2. Characterization

Nitrogen adsorption–desorption isotherms were obtained with an ASAP-2010 (Micromeritics) instrument, and pore size distributions were determined by the BJH (Barret–Joyner–Hallender) method applied to the desorption branch of the nitrogen isotherm. Nickel dispersion and carbon deposition on the supported catalysts were examined by transmission electron microscopy (TEM) analyses (Jeol, JEM-2000EXII). The crystalline phases of supports and supported catalysts were investigated by XRD (X-ray diffraction) (MAC Science, M18XHF-SRA) measurements using Cu Kα radiation ($\lambda = 1.54056$ Å) operated at 50 kV and 100 mA. In order to examine the reducibility of supported catalysts, temperature-programmed reduction (TPR) measurements were carried out in a conventional flow system with a moisture trap connected to a thermal conductivity detector (TCD) at temperatures that ranged from room temperature to 1000 °C with a ramping rate of 5 °C min^{-1}. For TPR measurements, a mixed stream of H_2 (2 ml min^{-1}) and N_2 (20 ml min^{-1}) was used for 0.1 g of catalyst sample. The chemical states of alumina supports were examined by ^{27}Al MAS NMR (magic angle spinning nuclear magnetic resonance) analyses (AVANCE, 400WB).

2.3. Steam reforming of LNG

Steam reforming of LNG was carried out in a continuous flow fixed-bed reactor at atmospheric pressure. Each calcined catalyst (100 mg) was charged into a tubular quartz reactor, and it was then reduced with a mixed stream of H_2 (3 ml min^{-1}) and N_2 (30 ml min^{-1}) at 700 °C for 3 h. Water was sufficiently vapourized by passing through a pre-heating zone and continuously fed into the reactor together with LNG (92.0 vol.% CH_4 and 8.0 vol.% C_2H_6) and N_2 carrier (30 ml min^{-1}). The steam:carbon ratio in the feed stream was fixed at 2.0, and the total feed rate with respect to the catalyst was maintained at 27 000 ml h^{-1} g^{-1}. The catalytic reaction was carried out at 600 °C. The reaction products were sampled periodically and analyzed using an on-line gas chromatograph (Younglin, ACME 6000) equipped with a TCD (thermal conductivity detector). LNG conversion was calculated according to the following equation on the basis of carbon balance:

$$\text{LNG conversion}\,(\%) = \left(1 - \frac{F_{CH_4,\text{out}} + F_{C_2H_6,\text{out}}}{F_{CH_4,\text{in}} + F_{C_2H_6,\text{in}}}\right) \times 100 \quad (1)$$

3. Results and discussion

3.1. Textural property of supports and supported catalysts

Textural properties of the A-SG support and the Ni/A-SG catalyst were examined by nitrogen adsorption–desorption isotherm measurements. Fig. 1 shows the nitrogen

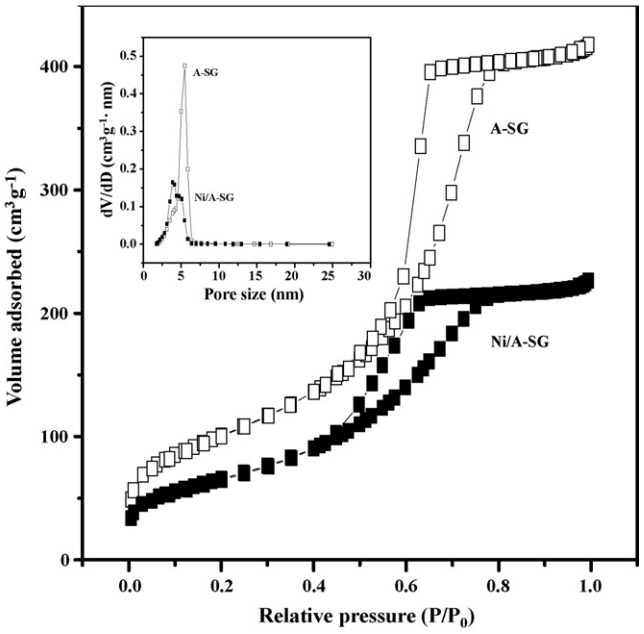

Fig. 1. Nitrogen adsorption–desorption isotherms and pore size distributions of A-SG support and Ni/A-SG catalyst.

adsorption–desorption isotherms and pore size distributions of the A-SG support and the Ni/A-SG catalyst. Both A-SG and Ni/A-SG samples clearly yield IV-type isotherms with H_2 hysteresis loops. This indicates the existence of 'ink bottle' pores with a narrow entrance and a large cavity. Both the A-SG support and the Ni/A-SG catalyst have well-developed framework mesopores with a narrow pore size distribution. The average pore sizes of the A-SG support and the Ni/A-SG catalyst are 4.7 and 4 nm,respectively.

Detailed textural properties of supports (A-C and A-SG) and supported catalysts (Ni/A-C and Ni/A-SG) are summarized in Table 1. The alumina xerogel support (A-SG) retained a higher surface area and a larger pore volume than the commercial alumina support (A-C). Furthermore, the Ni/A-SG catalyst had a higher surface area and a larger pore volume than the Ni/A-C catalyst. The Ni/A-SG catalyst showed a lower surface area and a smaller pore volume than the A-SG support, due to the pore blocking by the nickel species that had occurred during the impregnation step. The Ni/A-C catalyst also showed a lower surface area than the A-C support, but exhibited a larger pore volume and a larger pore size than the A-C support, even though the Ni/A-C catalyst was also prepared by impregnating a nickel precursor on the A-C support. This may be explained by the nature of A-C. The A-C support consists of non-porous nanoparticles, and its pore volume and pore diameter are attributed to the pores formed from some aggregates of these nanoparticles. It is concluded that the nickel species employed in the impregnation step play the role of a chemical glue for the A-C nanoparticles. Therefore, a number of large pores would be formed by the action of this chemical glue upon impregnation of the nickel species on the A-C support, leading to an increase in pore volume of the Ni/A-C catalyst [32].

Table 1
Textural properties of supports (A-C and A-SG) and supported catalysts (Ni/A-C and Ni/A-SG)

Sample	Surface area ($m^2\ g^{-1}$)[a]	Pore volume ($cm^3\ g^{-1}$)[b]	Average pore size (nm)[c]
A-C	95	0.25	12.5
A-SG	365	0.64	4.7
Ni/A-C	82	0.30	17.0
Ni/A-SG	238	0.34	4.0

[a] Calculated by BET (Brunauer–Emmett–Teller) equation.
[b] BJH (Barret–Joyner–Hallender) desorption pore volume.
[c] BJH (Barret–Joyner–Hallender) desorption average pore diameter.

3.2. Crystal structure and phase of A-C and A-SG supports

Fig. 2 shows the XRD patterns of A-C and A-SG supports calcined at 700 °C for 5 h. The A-C support displays the characteristic diffraction peaks of γ-Al_2O_3. By contrast, the A-SG support shows an amorphous feature even after the calcination at 700 °C. It is known that the phase of alumina is transformed from boehmite (AlOOH) to γ-Al_2O_3 at temperatures above 500 °C [33,34]. The experimental results indicate that the hydroxyl-rich surface properties of the alumina xerogel retard the aggregation of alumina particles which causes a phase transformation during the heat-treatment step.

In order to identify the accurate phases of A-C and A-SG supports, ^{27}Al MAS NMR analyses were conducted. Fig. 3 shows the ^{27}Al MAS NMR spectra of A-C and A-SG supports. The A-C supports show two different types of stable Al atoms, including 4-coordinated Al atoms (Al^{IV}) and 6-coordinated Al atoms (Al^{VI}). This result is in good agreement with the reported coordination numbers of γ-Al_2O_3 [35–37]. On the other hand, the A-SG support shows three coordination states of Al atoms, including Al^{IV}, Al^{V}, and Al^{VI}. It is noteworthy that 5-coordinated Al atoms (Al^{V}) appear in the A-SG support even after thermal treatment at a high temperature of 700 °C. It has been reported that the 5-coordinated Al atoms (Al^{V}) are formed during the course of transformation

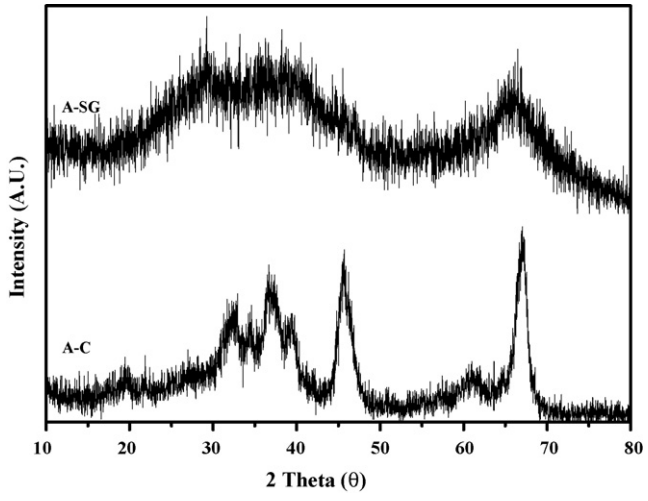

Fig. 2. XRD patterns of A-C and A-SG supports calcined at 700 °C for 5 h.

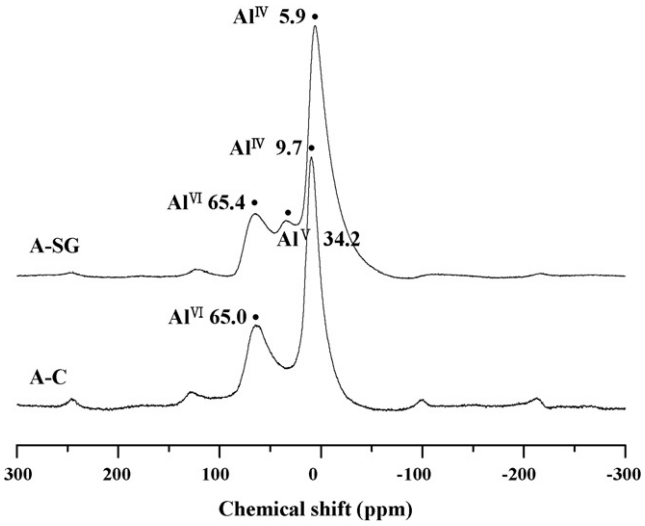

Fig. 3. ^{27}Al MAS NMR spectra of A-C and A-SG supports.

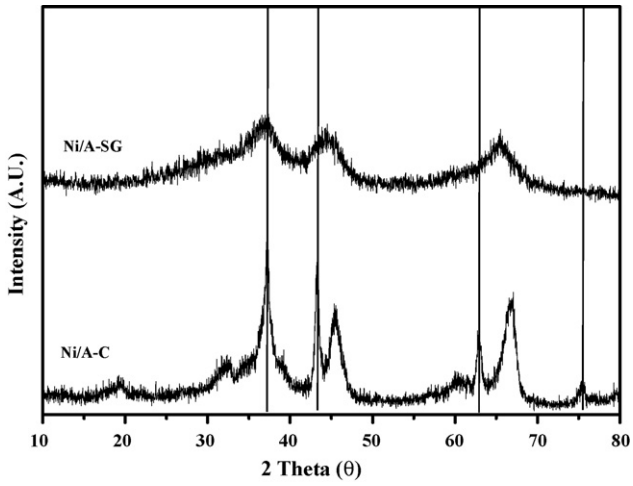

Fig. 4. XRD patterns of Ni/A-C and Ni/A-SG catalysts calcined at 700 °C for 5 h.

of Al atoms in the alumina xerogel into either 4-coordinated Al atoms (Al^{IV}) or 6-coordinated Al atoms (Al^{VI}) [37,38]. The 5-coordinated Al atoms (Al^{V}) in the A-SG support serve as an electron acceptor (Lewis acid), resulting in the formation of many electron-deficient sites in the A-SG support [39]. It is considered that the large amount of electron-deficient sites in the A-SG support would be favourable for the fine dispersion of the nickel species in the Ni/A-SG catalyst.

3.3. Nickel dispersion on Ni/A-C and Ni/A-SG catalysts

Fig. 4 shows the XRD patterns of Ni/A-C and Ni/A-SG catalysts calcined at 700 °C for 5 h. No diffraction peaks that are characteristic of nickel oxides are observed in the Ni/A-SG catalyst. This indicates that the nickel species are finely dispersed on the surface of the A-SG support and thereby result in the formation of small nickel particles that are below the detection limit of XRD measurements. It is likely that the 5-coordinated Al atoms (Al^{V}) in the A-SG support greatly enhance the incorporation of the nickel species into the support. It is also thought that the nickel species are highly dispersed on the hydroxyl-rich surface of the A-SG support. The finely dispersed nickel species would exist as a bulk nickel aluminate phase or a surface nickel aluminate phase due to the calcination at high temperature. On the other hand, both nickel oxide species (solid lines) and nickel aluminate species are observed in the Ni/A-C catalyst. The above result indicates that the dispersion of nickel species on the A-C support is relatively poor. The dispersion of nickel species in both catalysts is further confirmed by TEM analyses. Fig. 5 presents TEM images of Ni/A-C and Ni/A-SG catalysts calcined at 700 °C for 5 h. The Ni/A-C catalyst show large nickel species compared with the Ni/A-SG catalyst. It is clearly seen that the nickel species are finely dispersed on the A-SG support.

3.4. Reducibility of Ni/A-C and Ni/A-SG catalysts

TPR measurements were carried out to investigate the reducibility of the Ni/A-C and Ni/A-SG catalysts and to examine the interaction between nickel species and supports. Fig. 6 gives TPR profiles of the two catalysts. The Ni/A-C catalyst shows two reduction bands at around 420 and 820 °C. The minor

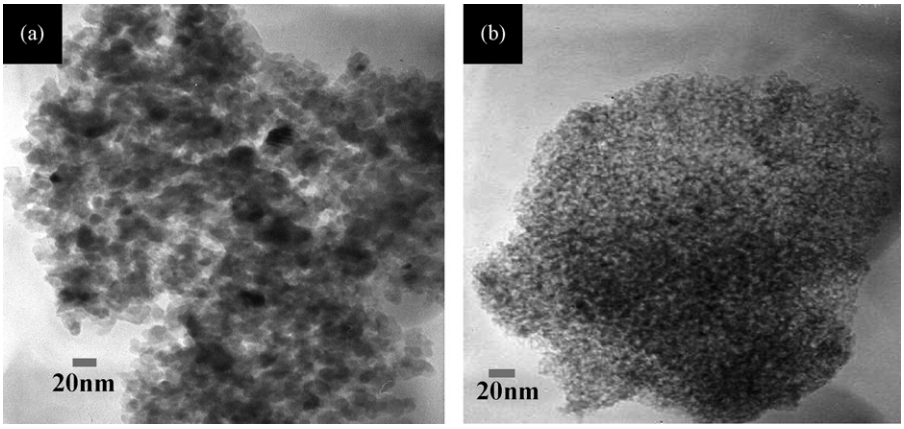

Fig. 5. TEM images of (a) Ni/A-C and (b) Ni/A-SG catalysts calcined at 700 °C for 5 h.

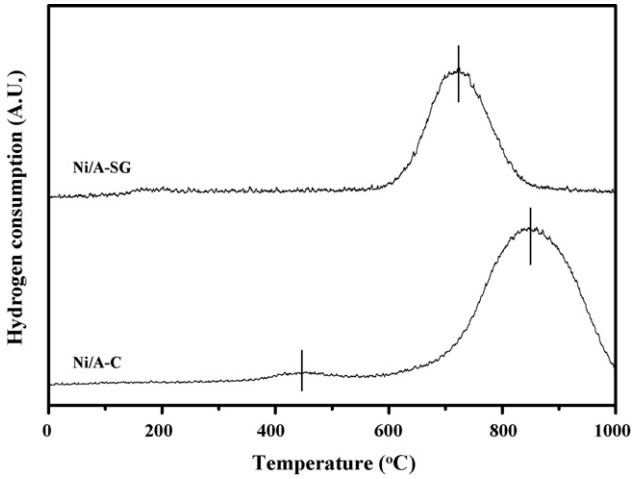

Fig. 6. TPR profiles of Ni/A-C and Ni/A-SG catalysts.

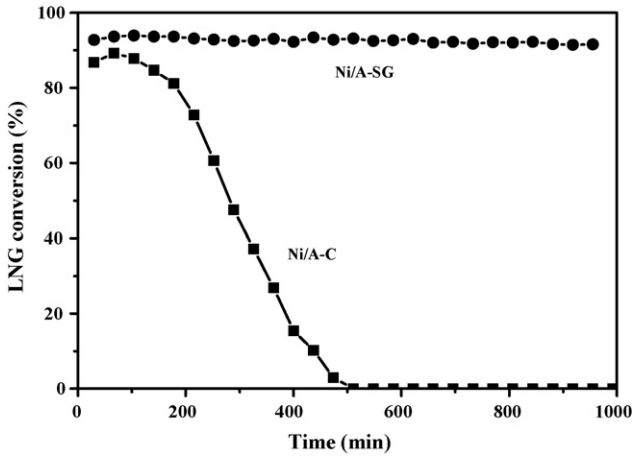

Fig. 7. LNG conversions with time on stream in steam reforming of LNG over Ni/A-C and Ni/A-SG catalysts at 600 °C.

reduction band appearing at the lower temperature is attributed to reduction of the bulk NiO species, while the major reduction band appearing at the higher temperature is due to reduction of the bulk nickel aluminate phase. It is well known that the latter phase is hard to reduce because Ni^{2+} ions are incorporated into the lattice of bulk γ-Al_2O_3. On the other hand, the Ni/A-SG catalyst displays one reduction band at around 710 °C, which is due to the reduction of the surface nickel aluminate phase. A direct comparison of the major reduction bands in the two catalysts reveals that the Ni/A-SG catalyst retains a higher reducibility than the Ni/A-C catalyst. These results indicate that the finely dispersed nickel species in the Ni/A-SG catalyst exist mainly as a surface nickel aluminate phase, which is easier to reduce than the bulk nickel aluminate phase [40–42]. The surface nickel aluminate phase has an intermediate reducibility between bulk nickel aluminate and bulk nickel oxide, and at the same time, has a relatively excellent stability due to its aluminate nature.

3.5. Steam reforming of LNG over Ni/A-C and Ni/A-SG catalysts

The LNG conversion with time on stream in steam reforming over Ni/A-C and Ni/A-SG catalysts at 600 °C is given in Fig. 7. The Ni/A-C catalyst experiences a severe catalyst deactivation, while the Ni/A-SG catalyst maintains a stable catalytic performance during the reaction extending over 1000 min. The reasons why the Ni/A-SG catalyst yields better catalytic performance can be explained in terms of chemical and textural properties of the A-SG support. One possible reason is attributed to the high reducibility of the Ni/A-SG catalyst (Fig. 6). Although the reducibility of a catalyst is not the sole factor determining catalytic performance, by retaining a higher reducibility the Ni/A-SG catalyst exhibits a better catalytic performance than the Ni/A-C catalyst. It is also thought that many electron-deficient sites that originate from 5-coordinated Al atoms (Al^V) in the A-SG support enhance the dispersion of nickel species by form-

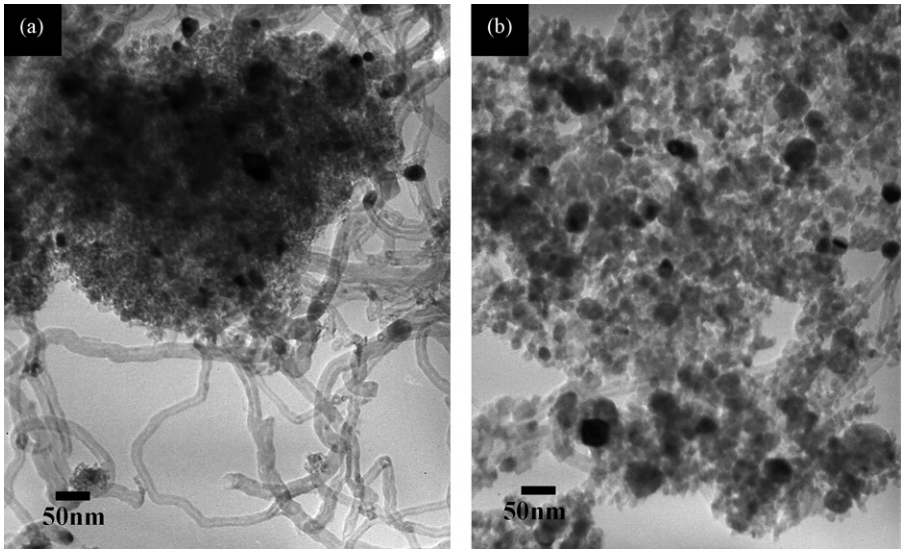

Fig. 8. TEM images of (a) Ni/A-C and (b) Ni/A-SG catalysts after a 1000-min reaction.

ing a surface nickel aluminate phase in the Ni/A-SG catalyst. The surface nickel aluminate phase, in turn, increases the active surface area of nickel. Another possible reason for the enhanced catalytic performance of Ni/A-SG may be due to the favourable textural structure of the A-SG support. The high surface area and the well-developed mesoporosity of the Ni/A-SG catalyst enhance gasification of the adsorbed surface hydrocarbons in the steam reforming reaction.

Hydrogen production by the steam reforming of methane is closely related to the following two adsorption mechanisms. One is the dissociative adsorption of methane on the active nickel surface, and the other is the dissociative adsorption of steam on either the active nickel surface or the support [43]. Nickel-based catalysts activate both the steam reforming reaction and the carbon formation reaction on the catalyst surface [44]. The gasification reaction can be preferentially enhanced, however, by increasing dispersion of active nickel on the catalyst surface.

TEM images of the Ni/A-C and Ni/A-SG catalysts after a 1000-min reaction are given in Fig. 8. The used Ni/A-C catalyst shows filamentous carbon that is derived from the dissolved carbon on the active nickel surface. CHNS elemental analyses reveal that the catalyst contains 12 wt.% carbon species after a 1000-min reaction. At the initial stage of reaction, the amount of dissolved carbon is too small to affect greatly the catalytic performance of the Ni/A-C. Nevertheless, the amount of dissolved carbon increases and the carbon filament is gradually formed as the reaction proceeds, which results in severe deactivation of the Ni/A-C catalyst (Fig. 7). By comparison, the used Ni/A-SG catalyst shows no significant formation of filamentous carbon. The amount of carbon species deposited on the Ni/A-SG catalyst after a 1000-min reaction is 2.7 wt.%. The carbon deposition preferentially occurs on the surface of large nickel particles. Small nickel particles on the Ni/A-SG catalyst, therefore, have a relatively strong resistance towards carbon deposition.

The H_2 compositions in the dry gas with time on stream in the steam reforming of LNG over Ni/A-C and Ni/A-SG catalysts at 600 °C are presented in Fig. 9. The H_2 compositions (Fig. 9) exhibit a similar trend to LNG conversions (Fig. 7) over both catalysts with time on stream. The steam reforming of methane is expressed as follows:

$$CH_4 + H_2O \rightarrow CO + 3H_2, \quad \Delta H_{298\,K} = 206\,kJ\,mol^{-1} \qquad (2)$$

A simple calculation shows that 75% hydrogen (dry gas basis) can be obtained in the steam reforming of methane under the condition of complete reaction. As shown in Fig. 9, the Ni/A-SG catalyst produced ca. 70% hydrogen (dry gas basis), a slightly lower value than the theoretical estimate. It is concluded that the A-SG support prepared by a sol–gel method serves as an efficient support for the nickel catalyst in hydrogen production by the steam reforming of LNG.

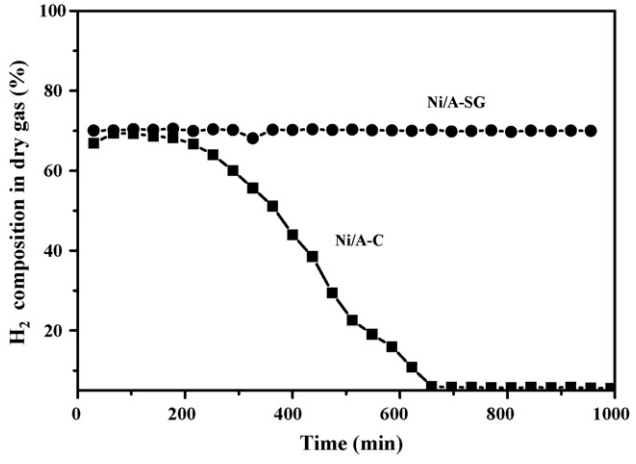

Fig. 9. Hydrogen compositions in dry gas with time on stream in steam reforming of LNG over Ni/A-C and Ni/A-SG catalysts at 600 °C.

4. Conclusions

Mesoporous alumina xerogel (A-SG) has been prepared by a sol–gel method. A Ni/A-SG catalyst has then been prepared by an impregnation method for use in hydrogen production by the steam reforming of LNG. The effect of the mesoporous alumina xerogel support on the catalytic performance of Ni/A-SG has been investigated. For the purpose of comparison, a nickel catalyst supported on commercial alumina (A-C) has also been prepared by an impregnation method (Ni/A-C). The A-SG support serves as an efficient support for the nickel catalyst in the steam reforming of LNG. The 5-coordinated Al atoms (Al^V) of the A-SG support play an important role in forming more electron-deficient sites on the support. Experimental findings reveal that both the hydroxyl-rich surface and the electron-deficient sites of the A-SG support enhance the dispersion of nickel species on the support through the formation of a surface nickel aluminate phase. The surface nickel aluminate phase of the Ni/A-SG catalyst increases the reducibility and stability of the catalyst. The Ni/A-SG catalyst shows a better catalytic performance than the Ni/A-C catalyst in terms of LNG conversion and hydrogen production. The high surface area and the well-developed mesoporosity of the Ni/A-SG catalyst enhance the gasification of adsorbed surface hydrocarbons in the stream reforming of LNG. Unlike the Ni/A-C catalyst, the Ni/A-SG catalyst shows strong resistance toward catalyst deactivation. It is concluded that the A-SG support prepared by a facile sol–gel method serves as an efficient support for the nickel catalyst in hydrogen production by steam reforming of LNG.

Acknowledgements

The authors wish to acknowledge support from the Seoul Renewable Energy Research Consortium (Seoul R & BD Program) and the Research Center for Energy Conversion and Storage (R11-2002-102-00000-0).

References

[1] J.N. Armor, Appl. Catal. A 176 (1999) 159.
[2] S.W. Nahm, S.P. Youn, H.Y. Ha, S.-A. Hong, A.P. Maganyuk, Korean J. Chem. Eng. 17 (2000) 288.
[3] K.J. Lee, D. Park, Korean J. Chem. Eng. 15 (1998) 658.
[4] K.D. Ko, J.K. Lee, D. Park, S.H. Shin, Korean J. Chem. Eng. 12 (1995) 478.
[5] J.R. Rostrup-Nielsen, J. Sehested, J.K. Norskov, Adv. Catal. 47 (2002) 65.

[6] J.R. Rostrup-Nielsen, Catal. Today 63 (2000) 159.
[7] J. Sehested, J.A.P. Gelten, I.N. Remediakis, H. Bengaard, J.K. Nørskov, J. Catal. 223 (2004) 432.
[8] S.C. Tsang, J.B. Claridge, M.L.H. Green, Catal. Today 23 (1995) 3.
[9] A.C.S.C. Teixeira, R. Giudici, Chem. Eng. Sci. 56 (2001) 789.
[10] Z.-W. Liu, K.-W. Jun, H.-S. Roh, S.-E. Park, J. Power Sources 111 (2002) 283.
[11] T. Takeguchi, Y. Kani, T. Yano, R. Kikuchi, K. Eguchi, K. Tsujimoto, Y. Uchida, A. Ueno, K. Omoshiki, M. Aizawa, J. Power Sources 112 (2002) 588.
[12] Q. Ming, T. Healey, L. Allen, P. Irving, Catal. Today 77 (2002) 51.
[13] H.-S. Roh, K.-W. Jun, S.-E. Park, Appl. Catal. A 251 (2003) 275.
[14] A. Vargas, C. Maldonado, J.A. Montoya, L. Norena, J. Morales, Appl. Catal. A 273 (2004) 269.
[15] L. Kepinski, B. Stasinska, T. Borowiecki, Carbon 38 (2000) 1845.
[16] R. Takahashi, S. Sato, T. Sodesawa, M. Yoshida, S. Tomiyama, Appl. Catal. A 273 (2004) 211.
[17] M.E.S. Hegarty, A.M. O'Connor, J.R.H. Ross, Catal. Today 42 (1998) 225.
[18] J.G. Seo, M.H. Youn, I.K. Song, J. Mol. Catal. A 268 (2007) 9.
[19] H.-S. Roh, K.-W. Jun, W.-S. Dong, J.-S. Chang, S.-E. Park, Y.-I. Joe, J. Mol. Catal. A 181 (2002) 137.
[20] S. Natesakhawat, R.B. Watson, X. Wang, U.S. Ozkan, J. Catal. 234 (2005) 496.
[21] T. Borowiecki, G. Wojciech, D. Andrzej, Appl. Catal. A 270 (2004) 27.
[22] T. Borowiecki, A. Goiebiowski, B. Stasinska, Appl. Catal. A 153 (1997) 141.
[23] J.S. Lisboa, D.C.R.M. Santos, F.B. Passos, F.B. Noronha, Catal. Today 101 (2005) 15.
[24] T.V. Choudhary, C. Sivadinarayana, D.W. Goodman, Chem. Eng. J. 93 (2003) 69.
[25] S. Tang, L. Ji, J. Lin, H.C. Zeng, K.L. Tan, K. Li, J. Catal. 194 (2000) 424.
[26] A. Valentini, N.L.V. Carreno, L.F.D. Probst, E.R. Leite, E. Longo, Micropor. Mesopor. Mater. 68 (2004) 151.
[27] S.C.E. Quincoces, E.I. Basaldella, S.P. De Vargas, M.G. Gonzalez, Mater. Lett. 58 (2004) 272.
[28] J.-H. Kim, D.J. Suh, T.-J. Park, K.-L. Kim, Appl. Catal. A 197 (2000) 191.
[29] Y. Zhang, G. Xiong, S. Sheng, W. Yang, Catal. Today 63 (2000) 517.
[30] D.J. Suh, T.-J. Park, J.-H. Kim, K.-L. Kim, J. Non-Cryst. Solids 225 (1998) 168.
[31] D.J. Suh, T.-J. Park, J.-H. Kim, K.-L. Kim, Chem. Mater. 9 (1997) 1903.
[32] P. Kim, Y. Kim, H. Kim, I.K. Song, J. Yi, Appl. Catal. A 272 (2004) 157.
[33] C. Kaya, F. Kaya, A.R. Boccaccini, K.K. Chawla, Acta Mater. 49 (2001) 1189.
[34] H.S. Santos, P.K. Kiyohara, P.S. Santos, Ceram. Int. 20 (1994) 175.
[35] M. McMillan, J.S. Brinen, G.L. Haller, J. Catal. 97 (1986) 243.
[36] C.S. John, N.C.M. Alma, G.R. Hays, Appl. Catal. 6 (1983) 341.
[37] Y. Kim, C. Kim, P. Kim, J. Yi, J. Non-Cryst. Solids 351 (2005) 550.
[38] X. Krokidis, P. Raybaud, A.-E. Gobichon, B. Rebours, R. Euzen, H. Toulhoat, J. Phys. Chem. B 105 (2001) 5121.
[39] F.R. Chen, J.G. Davis, J.J. Fripiat, J. Catal. 133 (1992) 263.
[40] M.L. Jacono, M. Schiavello, A. Cimino, J. Phys. Chem. 75 (1971) 1044.
[41] S. Narayanan, K. Uma, J. Chem. Soc., Faraday Trans. 81 (1983) 273.
[42] A.N. Kharat, P. Pendleton, A. Badalyan, M. Abedini, M.M. Amini, J. Catal. 205 (2002) 7.
[43] Y. Matsumura, T. Nakamori, Appl. Catal. A 258 (2004) 107.
[44] J.R. Rostrub-Nielson, D.L. Trimm, J. Catal. 48 (1977) 155.